FRACTURE MECHANICS BEHAVIOR OF HSS STEEL WELDED JOINT HETEROGENEOUS STRUCTURE - EXPERIMENTAL AND NUMERICAL EVALUATION

D. TOMERLIN*+, N. GUBELJAK**, D. KOZAK*, W. LI***, N. TRIŠOVIĆ****

**Mechanical Engineering Faculty, University of Slavonski Brod, HR-35000 Slavonski Brod, Croatia; 0000-0002-3461-4954*
dtomerlin@unisb.hr; 0000-0001-6542-0688 dkozak@unisb.hr; +corresponding author
***Faculty of Mechanical Engineering, University of Maribor, SI-2000 Maribor, Slovenia; 0000-0002-3276-8431*
****School of Mathematics and Statistics, Xidian University, Xi'an, P. R. of China; liweilw@mail.xidian.edu.cn*
*****Faculty of Mechanical Engineering, University of Beograd, 11120 Beograd, Serbia; 0000-0003-1043-5780*

DOI 10.3217/978-3-99161-089-2-021, license CC BY 4.0

ABSTRACT

Due to the physics and chemistry behind the fusion welding process, the welded joints are consequently significantly heterogeneous structures. They can be fundamentally divided into characteristic regions of Base Metal (BM), Weld Metal (WM) and Heat Affected Zone (HAZ). Such heterogeneity of the welded joint material microstructures in relation affects their general mechanical properties, which can vary significantly in relation to individual weld zones. The fracture behavior of welded joints consequently depends on the mechanical properties of the material zone in which the crack is located. The paper considers double-V butt joint (X joint) made of High Strength Steel (HSS), welded with filler metal having slightly overmatching mechanical properties as compared to base metal. The experimental work relies on the initial tensile testing in order to obtain stress-strain material properties, covering all the welded joint material regions of interest. In the continuation, the fracture mechanical testing is done to determine the fracture toughness characteristic parameters, as well as all the characteristic fracture behavior curves. The experimental investigation is carried out on Single Edge Notch Bend (SENB) specimens, located in welded joint zones of interest, namely BM, HAZ, and WM. The prediction of fracture behavior of metallic materials, through the initiation and evolution of damage, can be numerically simulated using the Ductile Damage material model. Such a model in general relies on stress-strain curves obtained from tensile tests of individual material zones within the observed heterogeneous structure. In this paper, using the example of SENB test specimens, the general methodology for modeling and simulating material heterogeneity of welded joints is presented. Finally, experimentally determined fracture mechanics curves and behavior of characteristic welded joint regions are simulated numerically for HSS steel grade. In this way, the possibility of numerically predicting the fracture behavior of heterogeneous structures is demonstrated.

Keywords: heterogeneous welded joint; high strength steel; fracture behavior; Ductile Damage model; numerical analysis

INTRODUCTION

Welded joints exhibit significant heterogeneity due to the complex thermal cycle involved in the welding process, which leads to the formation of multiple characteristic zones within the joint. During welding, localized melting occurs in specific regions, resulting in distinct microstructural changes and variations in material properties across these zones. The fundamental segmentation of a welded joint typically includes the base material (BM), the weld metal (WM), and the heat-affected zone (HAZ) [1,2]. The width of the HAZ is primarily influenced by the type of welding process employed as well as the specific process parameters, such as heat input, cooling rate, and welding speed. The boundary separating the HAZ from the base material is defined by the fusion line, which marks the transition from fully melted to thermally affected but non-melted material. Each of these zones is characterized by unique microstructures, such as different phases, grain sizes, and hardness levels, that directly affect the joint's overall mechanical properties, including strength, toughness, and ductility. The research on the topic of welded joint heterogeneity, its characteristic zones and related properties has been of significant interest to various researchers such as K.E. Easterling [1], E. F. Nippes [3], W. F. Savage et al. [4], J. C. Lippold [5], M. Lomozik [6] and others.

The heterogeneity of a welded joint is not only characterized by its division into main regions, the BM, HAZ and WM, but also through the strength mismatch within the joint. Welded joint strength mismatch refers to the differences in mechanical properties, especially yield strength, among these regions, focusing on the WM and BM. There are two primary types of mismatch: overmatching (OM), where the weld metal is stronger than the base metal, and undermatching (UM), where the weld metal is weaker. Each type uniquely affects stress distribution, crack initiation, and structural integrity. Weld strength mismatch is typically quantified by the ratio of yield strengths between the WM and BM, as expressed by the equation:

$$M = \frac{\sigma_{\mathrm{YW}}}{\sigma_{\mathrm{YB}}} \tag{1}$$

Where M is the mismatch factor, while σ_{YW} and σ_{YB} represent the yield strength of the WM and the yield strength of the BM, respectively.

The weld strength mismatch behavior is previously investigated by numerous researchers such as M. Koçak et al. [7], J. Spurrier et al. [8], Y. Lei and R. A. Ainsworth [9], Y. J. Kim and K. H. Schwalbe [10-12], G. H. B. Donato et al. [13], U. Zerbst et al. [14], and others. Heterogeneity in steel welded joints and strength mismatch effects, as the topics of research interest, are also being actively researched by the authors of this paper, D. Tomerlin, N. Gubeljak and D. Kozak [15,16].

Welded joint heterogeneity and strength mismatch significantly impact the fracture toughness and fracture behavior of welded steel structures. Variations in microstructure and mechanical properties across different weld zones (BM, WM and HAZ), create stress concentrations that can act as initiation sites for cracks. This microstructural heterogeneity influences crack propagation paths, potentially reducing toughness and increasing susceptibility to brittle fracture. Similarly, strength mismatch, whether OM or UM, affects stress distribution within the joint. OM welds have a WM with higher yield strength,

protecting the lower-toughness weld region from high strains that can lead to fracture during overload. While beneficial overall, OM can create a high triaxial stress state at the crack tip in the HAZ, potentially promoting local crack growth. UM welds have a lower yield strength WM, which offers higher ductility and toughness but can lead to faster fatigue crack growth and more significant deformation in the weld itself. Overall, these factors modulate the fracture toughness, crack initiation, and propagation characteristics of steel welds, highlighting the importance of understanding and controlling heterogeneity and mismatch to ensure structural integrity and safety.

The investigations outlined in this paper build upon a broader research effort by the authors, which focused on the heterogeneity of welded joints made from S690QL1 high-strength structural steel [15,16]. This prior work included developing methods and test specimens for experimental testing of small material zones within the welds [16,17], as well as conducting numerical modeling of heterogeneity within welded joints [16].

Specifically, the stress-strain properties of the heterogeneous welds were examined using Mini Tensile Specimens (MTS), and these findings were complemented by numerical simulations of several welded joint models (WJM) subjected to tensile testing, employing a ductile damage model. These preliminary studies: "*stress-strain properties of HSS steel welded joint heterogeneous structure: experimental and numerical evaluation*" published in "*Mathematical Modelling of Weld Phenomena 13*" [18], serve as the foundation for the current research presented here.

In scope of this paper, the acquisition of stress-strain data for the specific regions of interest: the BM, HAZ and WM, is done initially. Due to the limited size of these material regions, subsize tensile specimens are required. Suitable specimens for testing welded joints include Mini Tensile Specimens (MTS) and small-sized round specimens as specified in ASTM E8. The data obtained from these tensile tests are essential for developing and calibrating ductile damage numerical models.

Next, fracture mechanics testing following the ASTM E1820 standard is carried out to determine the fracture toughness parameters and to develop characteristic fracture behavior curves. These tests use Single Edge Notch Bend (SENB) specimens placed strategically in the weld joint regions of interest, including the BM, HAZ, and WM.

The second part of this paper focused on numerical modeling, initially proposes and establishes the welded joint geometry simplifications for numerical simulations purposes. Using these simplifications, the corresponding models of the SENB fracture test specimens are created specifically to simulate fracture behavior in the BM, HAZ, and WM regions of the welded joint. The fracture behavior, including damage initiation and progression curves, is accurately modeled with ABAQUS simulations utilizing the ductile damage material model. The numerical results are successfully matched with the experimental data, demonstrating the potential of numerical methods to predict the fracture behavior of heterogeneous welded structures.

MATERIALS AND EXPERIMENTAL METHODS

MATERIALS AND WELDED JOINT

This paper investigates a butt-welded X joint made from high-strength steel S690QL1, which constitutes the BM [19]. This fine-grained structural steel is produced through the quenching and tempering (QT) process, with a minimum declared yield strength $R_{p0.2} \geq 690$ MPa and a tensile strength R_m ranging from 770 to 840 MPa. The plates used in the welded test coupon are 40 mm thick, in accordance with the EN 10025-6 standard for hot rolled high yield strength structural steels in the QT condition. The fusion welding process, employs a high-strength ferritic filler, Mn3Ni1CrMo (ER110S-G), according to EN ISO 16834-A /AWS A5.28 standards, which constitutes the WM in the welded joint [20]. This filler material has a yield strength $R_{p0.2}$ of approximately 800 MPa and a tensile strength R_m ranging from 840 to 900 MPa.

In this welded joint, the calculated weld strength mismatch factor is $M = 1.16$, indicating the slightly OM weld metal.

The investigated welded test coupon consists of two 40 mm thick steel plates joined in a double V-butt (X-welded) configuration. The groove preparation was performed in accordance with the recommendations specified in EN ISO 9692-1, for joint reference No. 2.5.1, see Fig. 1 (a). Welding was executed using the metal active gas (MAG) 135 process with a 1.2 mm diameter solid filler wire. The shielding gas used was a mixture of 82% Argon and 18% CO2, with a flow rate of 12–16 L/min. The welding was performed in a multi-pass configuration, with a total of 22 passes, as shown in the Fig. 1 (b).

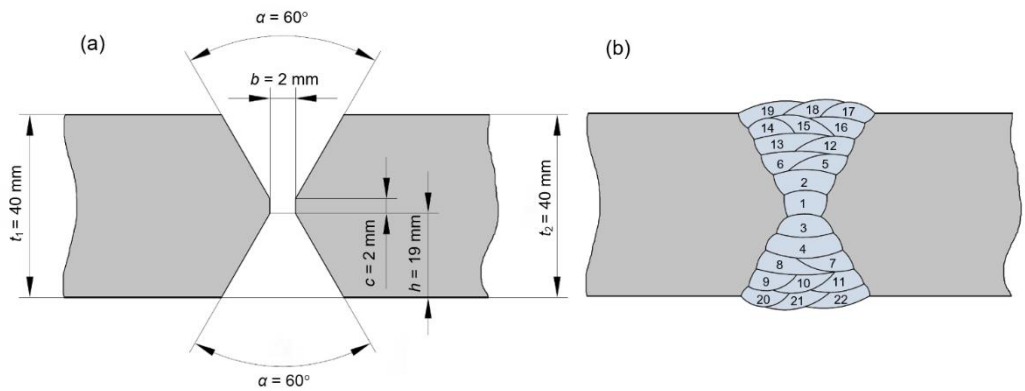

Fig. 1 X welded joint: (a) joint groove geometry and preparation, and (b) welding passes

To ensure high-quality weld with optimal performance and properties, the process parameters are adjusted to maintain low heat input, below 1 kJ/mm, as indicated in Table 1.

Table 1 Welding process parameters

Pass no.	Location	I [A]	U [V]	v_w [cm/min]	η	Q [kJ/mm]
1-3	root	195	26	28.5	0.8	0.85
4-22	fill + cover	280	29	45	0.8	0.87

TENSILE TESTING

To fully characterize the behavior and overall mechanical properties of a welded joint, it is essential to conduct experimental testing on each distinctive region of the heterogeneous weld structure and obtain required data for the following numerical simulations. Standard-sized tensile testing specimens often proposed and used in testing standards and welding codes are unsuitable for such small material volumes, making mechanical testing challenging or even unfeasible. In order to obtain the stress-strain properties of welded joint BM, HAZ and WM regions, the subsize or even miniature sized specimens are required.

As discussed in the introduction of this paper, the authors are investigating testing methods and specimen types suitable for evaluating heterogeneous welds [17], with particular emphasis on those relevant to this specific case:

- ASTM E8 round tensile subsize specimens, shown in Fig. 2 (a): suitable for testing welded joints on a general scale, allowing for the assessment of tensile properties in key segments such as the BM, HAZ, and WM. The specimens have a circular cross-section with a diameter D = 2.5 mm, resulting in a test area of 4.909 mm². However, method is not able to differentiate between specific sub regions within the HAZ, providing only the averaged values for this highly heterogeneos region.
- Mini Tensile Specimens (MTS), shown in Fig. 2 (b): suitable for complete linear characterizing the mechanical behavior of heterogeneous materials. When testing welded joints, this method is particularly valuable for measuring stress–strain properties across the weld's cross-sectional transverse line, with the ability to distinguish between the main segments of the weld, the BM, WM, and individual HAZ sub regions. The specimen has a rectangular cross-section with a width W = 2 mm and thickness T = 0.5 mm, resulting in a test area of 1 mm².

Given the requirement to determine the tensile properties of BM, WM and general HAZ regions, without deeper insights into the HAZ sub regions, the convenient testing method is ASTM E8 round tensile subsize specimens. For the regions of BM and WM the standard sized round tensile specimens can also be used. Test methods for all-weld metal (AWM) are given in EN ISO 15792-1 standard. Generally, the larger the test area covered by the specimen, the more averaged the results will be of the overall properties within the tested region.

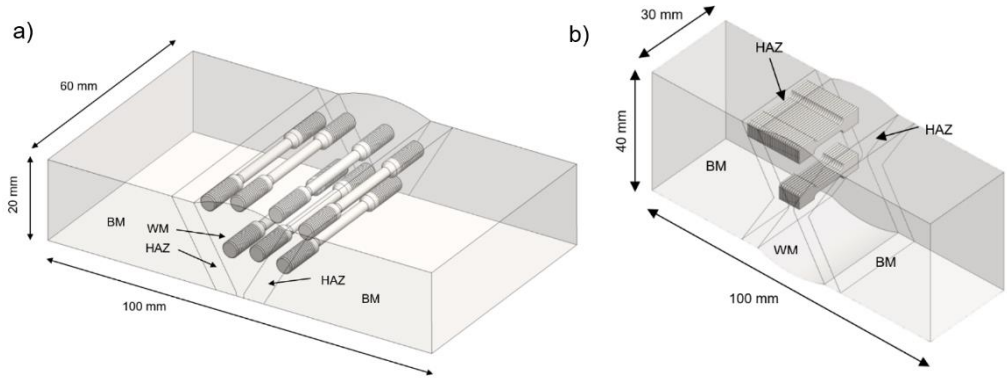

Fig. 2 Tensile testing methods for heterogeneous welds: (a) ASTM E8 round tensile subsize specimens and (b) Mini Tensile Specimens (MTS)

In case of ASTM E8 testing, 7 round tensile subsize specimens are proposed for welded joint testing, as shown in Fig. 2 (a). WM testing uses three specimens: two in the WM Fill zone and one in the WM Root zone, while 4 specimens are used for HAZ testing. The 3 additional subsize specimens (not illustrated in the figure) are used to test the BM through its 40 mm thickness.

Stress-strain curves are obtained for each tested specimen, while three region representative curves (Fig. 3) are shown and color-coded: BM in yellow, HAZ in blue, and WM in red tones. Results determined for BM the average yield strength $R_{p0.2}$ = 735 MPa, and average tensile strength R_m = 810 MPa, for WM the $R_{p0.2}$ = 780 MPa and R_m = 900 MPa, while for HAZ the $R_{p0.2}$ = 860 MPa and R_m = 940 MPa. Overall strength values trendline is generally moving from BM to WM an finally to HAZ.

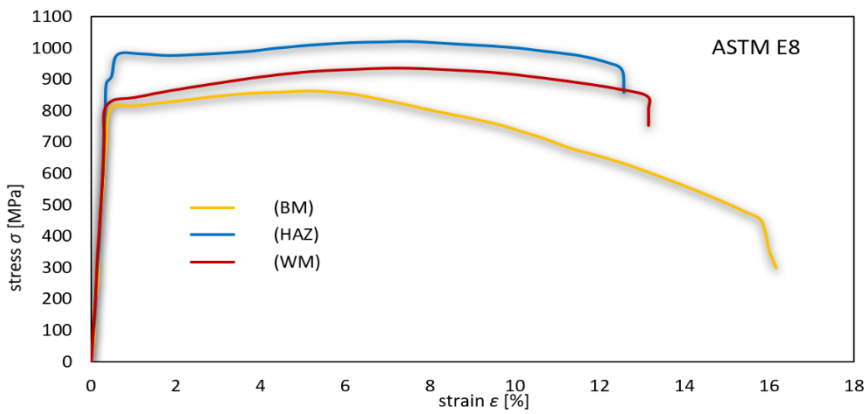

Fig. 3 ASTM E8 round tensile subsize specimens stress-strain curves

Tensile properties across the transverse line of X weld are determined using two sets of MTS, as shown in Fig. 2 (b). The top set (25 specimens: R1-R24 and R25 at the centerline), characterizes the fill-pass WM (Fill), HAZ, and BM. The central set (10 specimens: C1-C9 and C10 at the centerline), characterizes the root-pass WM (Root), HAZ, and BM. MTS are manufactured using the Electrical Discharge Wire Cutting (EDWC) technology, with the wire diameter 0.25 mm, which also dictates the lateral distance between the test specimens.

After testing, the corresponding σ–ε curves are also constructed for each tested MTS specimen, in fill pass Fig. 4 (a) and root pass Fig. 4 (b). Again, the σ–ε curves are color coded: BM in yellow, HAZ in blue, and WM in red tones. BM has lowest averaged strength $R_{p0.2} \approx$ 750 MPa and $R_m \approx$ 840 MPa, WM has $R_{p0.2} \approx$ 790 MPa and $R_m \approx$ 860 MPa, while HAZ has highest strength $R_{p0.2} \approx$ 840 MPa and $R_m \approx$ 900 MPa.

In general, for FEA input, either ASTM E8 or MTS results may be used. The averaged experimental stress–strain curves corresponding to the SENB specimen's location within weld regions are applied. The material data used in this study is obtained using MTS testing, and given later in Table 5.

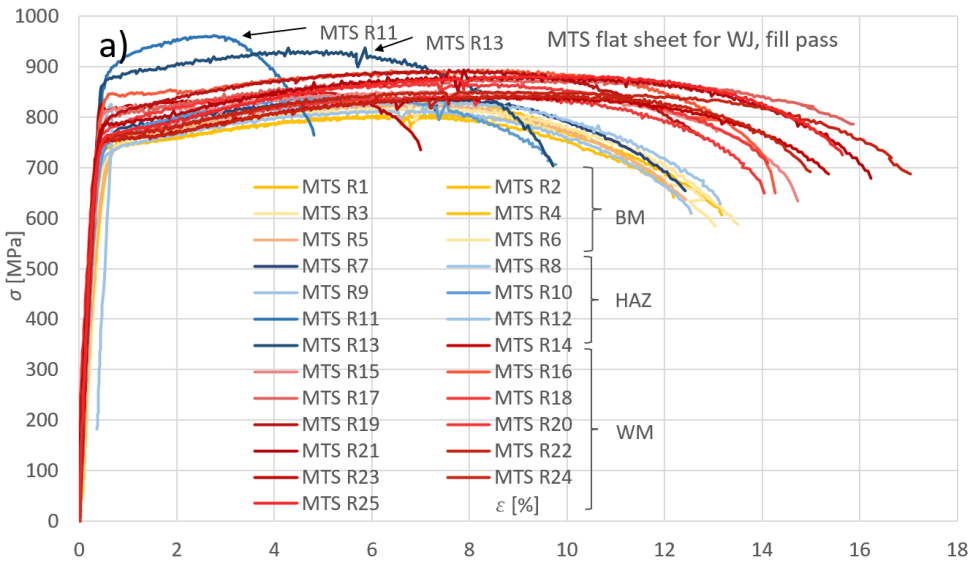

Fig. 4 MTS flat sheet subsize specimens stress-strain (σ–ε) curves, a) Fill pass

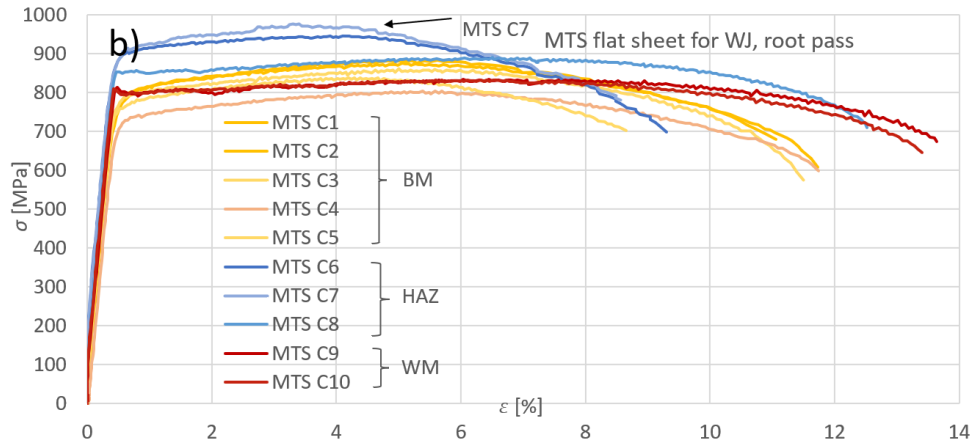

Fig. 4 MTS flat sheet subsize specimens stress-strain (σ–ε) curves, b) Root pass

FRACTURE TESTING

Fracture mechanics testing according to ASTM E1820 standard is performed to evaluate the fracture toughness characteristic parameters, and determine fracture behavior curves (e.g *P*-CMOD curves). Major regions of the X welded joint, the BM, HAZ, and WM are tested. To test these specific areas, the SENB specimens are positioned within the volume of the welded joint. The placement of the specimens and the locations of the notches were selected based on the general guidelines provided in BS 7448: Part 2. This arrangement of SENB specimens within the X weld joint main regions is illustrated in Fig. 5.

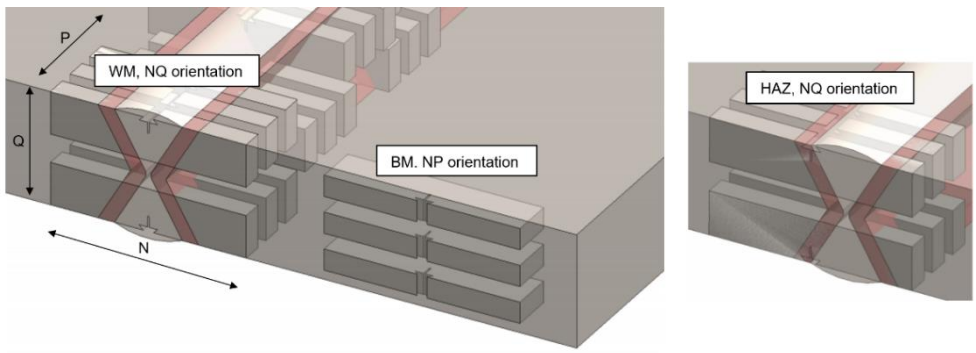

Fig. 5 Fracture mechanics testing - SENB specimens placement in welded joint BM, HAZ and WM

Based on BS 7448: Part 2, which specifies the crack plane orientation codes for welded fracture toughness specimens, the specimen codes used are: NP (crack opening in the N direction and propagation in P) and NQ (crack opening in the N direction and propagation in Q). Tested SENB specimen configurations are listed in Table 2.

Table 2 SENB specimens placement, orientation and initial crack location

SENB Specimen	Welded Joint Zone	Orientation	Crack
1	BM	NP	Crack initiation and through BM
2	WM	NQ	Crack initiation and through columnar WM, weld centre line
3	HAZ	NQ	Crack initiation in HAZ

The SENB fracture mechanics testing specimens are chosen and manufactured in relation to ASTM E1820. SENB specimens have dimensions of W = 15 mm, B = 7.5 mm, and a total length of 70 mm. The fatigue crack starter notch geometry, is a narrow notch type, being cut using the electrical discharge wire cutting (EDWC) with a wire diameter of 0.3 mm.

Fracture testing procedure in accordance with the ASTM E1820 standard, implies the initial fatigue precracking, starting from the fatigue crack starter notch. Three-point bending SENB specimens are cyclically loaded using the servo-hydraulic testing machine INSTRON 1255, with a load ratio R = 0.1, and applied $K_{max}/E \leq 1.1\times10^{-4}\text{m}^{1/2}$.

Fracture toughness tests are conducted next (Fig. 6), with crosshead displacement control at rate of 1.5 mm/min, at room temperature of 20°C. The fixture system includes two fixed bottom support rollers with a span distance of S = 58.7 and a top roller at the specimen's center. Top roller applies a downward load P ranging from 9 to 17.5 kN, depending on the individual specimen's resistance. All rollers have a diameter of R = 14 mm.

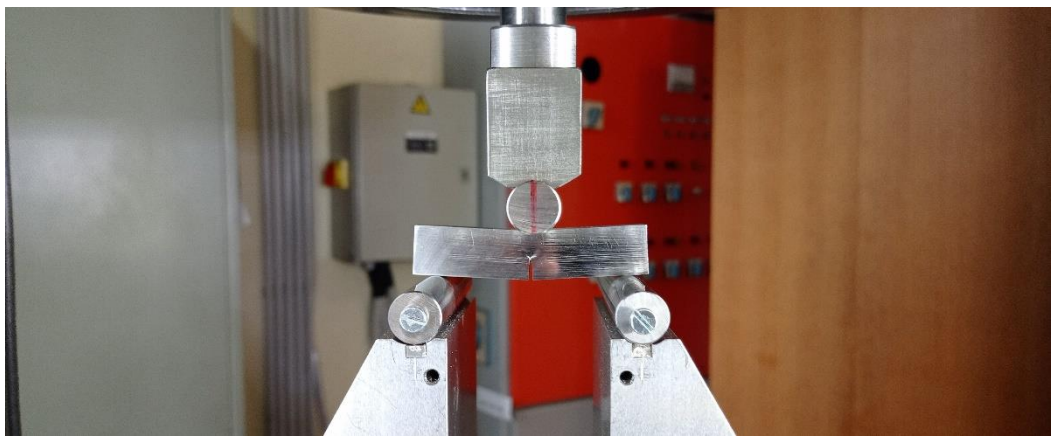

Fig. 6 Fracture mechanics testing - SENB specimens three-point bending

According to ASTM E1820, the fracture resistance is determined and characterized by J–R and CTOD(δ)–R curves. The fracture testing characteristic values are determined for three

designated weld zones (BM, WM and HAZ), where $J_{Q(1)}$ is *J*-Integral estimated value, K_{JIC} is Stress Intensity Factor (SIF) evaluated from *J*-Integral and $\delta_{Q(1)}$ is δ estimated value. Results are shown in Table 3.

Table 3 SENB specimens fracture toughness testing $J_{Q(1)}$, K_{JIC} and $\delta_{Q(1)}$

SENB Specimen	Welded Joint Zone	$J_{Q(1)}$ / J_{IC} [kJ/m^2]	K_{JIC} [MPa·m$^{1/2}$]	$\delta_{Q(1)}$ / δ_{IC} [mm]
1	BM	278	229	0.193
2	WM	165	181	0.120
3	HAZ	536	325	0.366

Observing the results, the HAZ is markedly tougher and more resistant to crack propagation, having highest energy absorption and opening displacement before fracture.

The experimental *P*-CMOD curves obtained from the experimental three-point bending testing SENB specimens, in comparison with numerically obtained curves, are shown later in Fig. 11.

NUMERICAL MODELLING OF WELDED JOINTS

SIMPLIFIED WELD MODEL

Given the geometric complexity and irregularity of welded joints, introducing simplifications in numerical modeling of these structures is essential. Some existing fracture behavior assessment procedures allow for the idealization of actual weld geometry, presenting the irregularities of the fusion line, as caused by individual welding passes, using straight lines. S. Hertelé et al. [21] previously proposed a methodology for simplifying and idealizing butt V welds, while P. Štefane et al. [22] extended this to simplified double-sided V welds (X welds). As a further development, the authors introduced a double linear idealization for the fusion lines and the boundary line separating the HAZ from the BM, as shown in Fig. 7.

The simplified model is superimposed on X joint macroscopic image, with extracted dimensions of interest: root zone width H_r = 2 mm, HAZ width H_{HAZ} = 2.5 mm and weld center height L_W = 20 mm, all with rounded values. Simplified model utilizes symmetry along both vertical and horizontal axes of the welded joint, with equal angles $\alpha = \beta = 60°$, resulting in identical upper and lower sides. In this study, the HAZ is treated as a uniform region, without sub-regional division. Welds with detailed HAZ segmentation are outside the scope of this paper, but were investigated by authors [16].

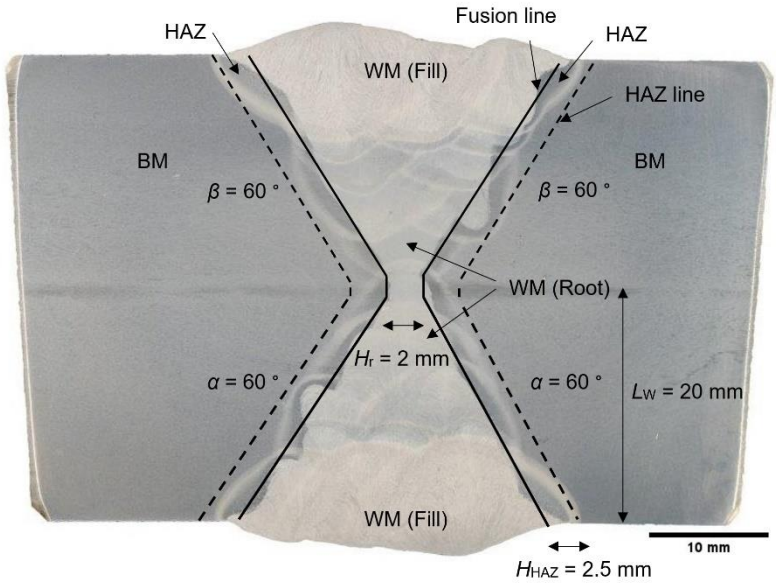

Fig. 7 X welded joint macrograph with simplified fusion and HAZ lines.

NUMERICAL MODELS - SENB SPECIMENS

Two-dimensional (2D) numerical model of the SENB test specimen and testing setup is developed, based on the modeling approaches for the specimen, notch, and crack previously used by P. Štefane et al. [22] and L. Starčevič et al. [23]. The authors also employed other modeling techniques for SENB specimens and cracks, as documented by various researchers in the literature [24–26]. All simulations are performed using ABAQUS software [27].

The comprehensive finite element (FE) model of the test setup includes both the SENB specimen and the three-point bending fixture system, as depicted in Fig. 6 (a). The fixture consists of two fixed bottom rollers (U1, U2, UR3 = 0), and one top roller having a prescribed vertical displacement (U2 ≠ 0), variable over time to simulate the applied load P. Rollers are modeled as analytical rigid bodies with a diameter of R = 14 mm.

The SENB specimen is modeled as a planar shell and fully discretized using a 4-node bilinear plane strain quadrilateral element CPE4R in an explicit FE analysis. The weld joint region is meshed with a structured or free mesh, with element sizes of 0.1. In regions outside the critical area, the mesh size is increased to 1 mm to optimize computational efficiency, as shown in Fig. 8 (a).

Notch is stage modelled as initial EDWC cut notch with length a_N and width of 3 FE, and fatigue precrack with length a_0, width of 1 FE, and blunt end, Fig. 8 (b). The numerically calculated results in ABAQUS, using the ductile damage model, are highly mesh-dependent. The accurate stress–strain fields at the notch tip require a well-refined mesh. In scope of this

investigation the intentionally simplified blunt notch is used, with fairly uniform mesh, giving adequate results and fast computations. In order to get the most accurate results, it is however recommended to use the sharp fatigue precrack tip combined with highly refined mesh at the notch tip itself.

The modelled zones are BM, WM and HAZ, using the MTS testing experimentally obtained tensile properties and corresponding ductile damage parameters, Fig. 8 (c-e).

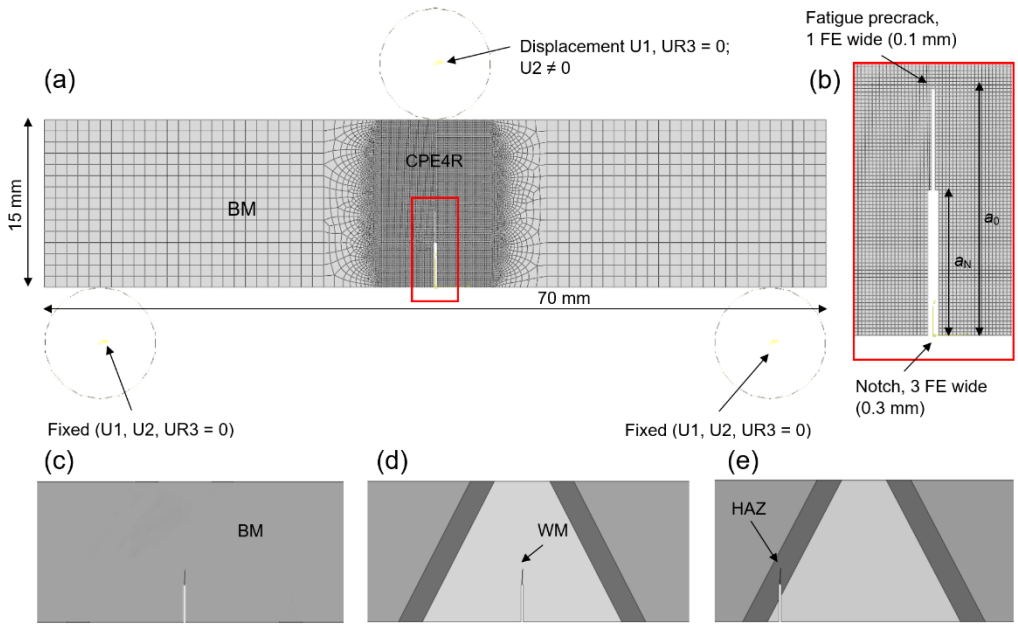

Fig. 8 Numerical models of SENB specimens: (a) bending test setup, (b) detail of notch and fatigue precrack, (c) BM specimen, (d) WM specimen and (e) HAZ specimen

DUCTILE DAMAGE MODEL

To model the behavior of elasto-plastic materials with progressive damage up to failure, the ABAQUS software with ductile damage model is employed. This model predicts damage initiation and evolution. The stress-strain curve (Fig. 9) depicts this progression: the initial linear-elastic stage (0a), followed by stable plastic deformation with strain hardening (ab). Point *b* marks the onset of plastic instability with damage parameter $D = 0$. Conversely, in the failure phase (bd), stiffness degradation and damage evolution occur, reaching $D = 1$ at point *d*, where crack initiation indicates failure [27,28].

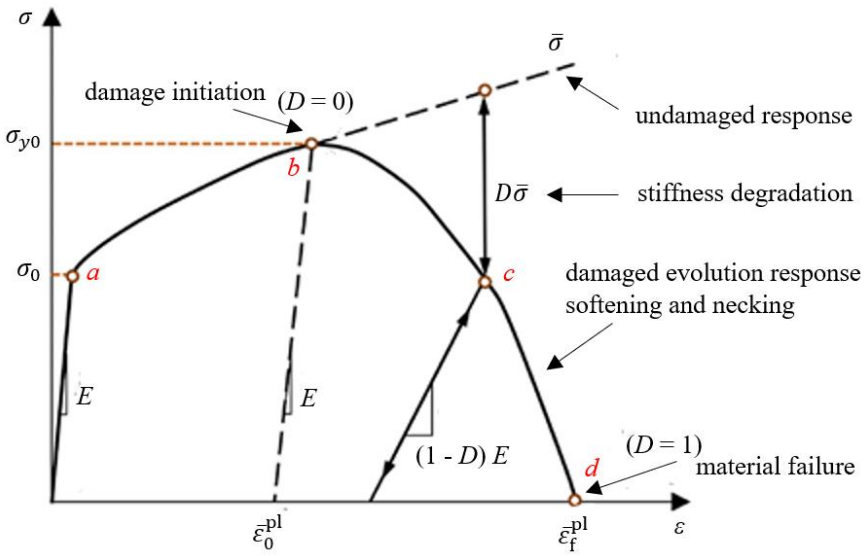

Fig. 9 Ductile damage model with stress-strain curve showing damage initiation and evolution [28]

The characteristic parameters in ductile damage model are:

- Damage parameter D, changing from 0 (non-damaged) to 1 (material failure).
- $\bar{\varepsilon}_{\mathrm{f}}^{\mathrm{pl}}$ equivalent plastic strain at failure, when the overall damage variable reaches the value $D = 1$
- $\bar{u}_{\mathrm{f}}^{\mathrm{pl}}$ [mm] damage evolution displacement at failure

The ductile damage model has previously been employed in simulations of the tensile behavior of flat sheet specimens, as part of the authors' earlier research published in "*Mathematical Modelling of Weld Phenomena 13*" [18]. Therefore, it will not be restated in this section.

Ductile damage model is readilly being used in numerical simulations for modelling the mismatching behavior of welded joints, as well as behavior of different types of test specimens, as provided in the relevant literature [23,29-32].

The redistribution of the plastic zone in mismatched welds plays a vital role in influencing fracture behavior. Plastic zone location, size, and shape are determined by local material properties, mismatch ratio, and residual stresses. Proper redistribution can either mitigate or exacerbate crack growth tendencies, as proposed by U. Zerbst [14,33,34].

The crack behavior in mismatched welds of high strength steel, using the SENB specimens, is investigated by the authors, and presented in Fig. 10. Material data and ductile damage parameters for the simulations, are provided in Table. 4.

Table 4 SENB specimens for mismatch welds, material data and ductile damage parameters

Specimen	Material	E	$R_{p0.2}$	R_m	M	$\bar{\varepsilon}_f^{pl}$	$\bar{u}_f^{pl}$	Δa	CMOD
		[GPa]	[MPa]	[MPa]			[mm]	[mm]	[mm]
SENB DD1	BM/WM	210/210	755/780	840/890	1.03	0.075/0.110	0.030/0.055	4.561	1.009
SENB DD2	BM/WM	210/210	690/780	770/890	1.13	0.090/0.110	0.025/0.200	1.722	1.004

In case of slight overmatching with M = 1.03, the crack growth is developing along the WM/BM boundary, as shown in Fig. 10 (a). On the other hand, in case of substantial overmatching with M = 1.13, the crack formed in the weaker BM, has the crack growth arrested on the WM transition front, as shown in Fig. 10 (b).

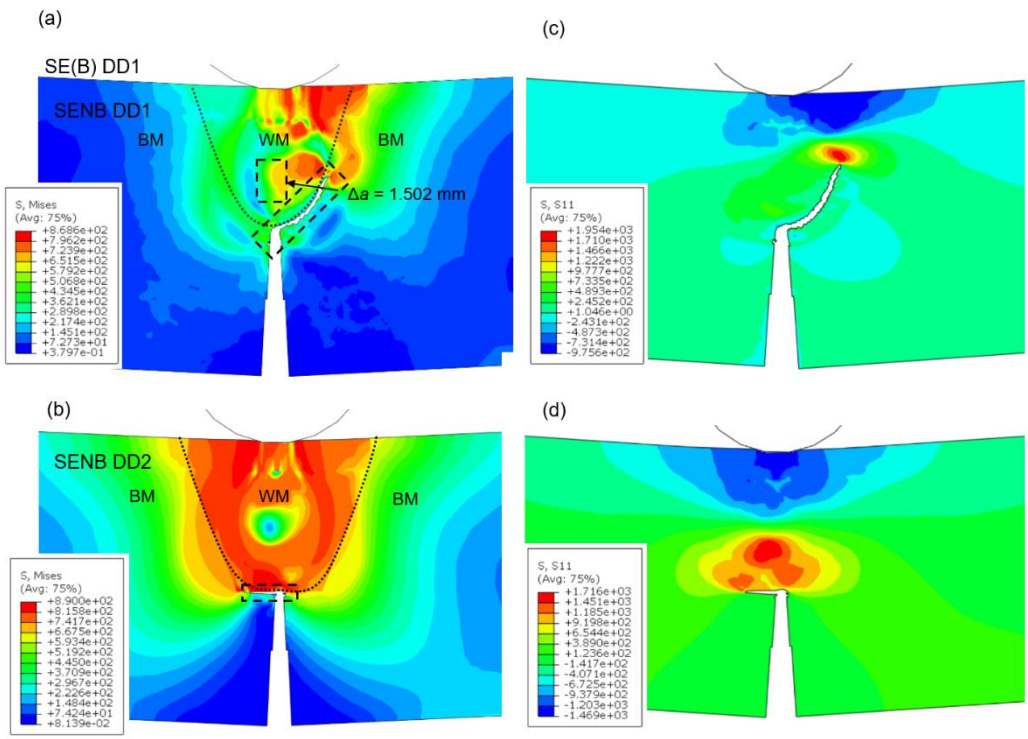

Fig. 10 SENB specimens for mismatch welds – damage behavior and crack growth: (a) SENB DD1 von Mises, (b) SENB DD2 von Mises, (c) SENB DD1 S11, (d) SENB DD2 S11

The colour stress contours shown in Fig. 10 (a, b) represent Von Mises stress fields, while the normal stress contours S11 are shown in Fig. 10 (c, d). Von Mises stress, being a scalar quantity (i.e. equivalent stress) that doesn't differentiate tension from compression, can misrepresent the stress state when strong compressive regions (under an indenter) coexist with tensile zones (at a crack tip). Tension and compression behavior is adressed using the S11

stress contour plots in Fig. 10 (c, d). The uncracked ligament acts as a plastic hinge, and undergoes gross plastic yielding rather than brittle crack propagation, causing plastic collapse of SENB specimen. This behavior is typical for ductile materials.

It is mandatory to note that numerical analysis of SENB DD1 and SENB DD2 is done just to showcase the specific crack behavior of different types of mismatched welds, having different material regions, related material parameters and ductile damage parameters. The actual experimental testing for those SENB specimens have not been done.

OM welds generally offer advantages under static loading, as the WM higher strength increases its resistance to applied stresses, delaying both crack initiation and growth. This results in enhanced performance and durability, with cracks tending to propagate through the HAZ or BM, as the stronger WM acts as a barrier and diverts crack paths. Conversely, UM welds are more prone to rapid crack initiation and growth, especially under cyclic loading, leading to stress concentrations that challenge the WM structural integrity. Cracks often initiate in the weaker WM and propagate linearly through the weld, increasing the risk of premature failure if not properly controlled [35].

In ductile damage model, the criteria for crack advancement is based on non self-similar crack growth, following the paths of localized plastic deformation. The crack advances in the direction where the elements reach the critical damage $D = 1$, being removed (i.e. deactivated) or have their stiffness set to near zero, forming a new traction-free surface. On the other hand, crack arrest will occur when the energy available for driving crack growth is less than the material's resistance, or when the damage process zone ceases to propagate.

Crack growth path is not typically constrained to move along the bimaterial interface simply because the material properties change abruptly. Instead, it is governed by local driving force vs. local material resistance. As damage accumulates, elements are softened or deleted. The crack follows the path of least resistance, where elements meet damage criteria first, causing them to lose stiffness (damage evolution) and fail, while the stronger material remains intact.

RESULTS AND DISCUSSION

FRACTURE BEHAVIOR SIMULATION

The fracture behavior, including damage initiation and progression curves for the BM, WM, and HAZ regions of the X welded joint, is simulated using ABAQUS with the ductile damage material model. The SENB specimens including these characteristic zones are modeled based on the previous numerical simplifications and the selected computational parameters, as previously described and shown in Fig. 8. The material data used for the simulations are obtained from experimental tensile MTS tests of the X weld (Fig. 4), using the averaged stress-strain curves depending on the specific test location inside the chosen material region (e.g. BM, WM, HAZ) and SENB placement location inside the weld. The ductile damage parameters are than calculated and assigned to each specimen accordingly, as summarized in Table 5.

Table 5 SENB specimens for BM, WM and HAZ, material data and ductile damage parameters

Specimen	Material	E [GPa]	$R_{p0.2}$ [MPa]	R_m [MPa]	$\bar{\varepsilon}_f^{pl}$	$\bar{u}_f^{pl}$ [mm]
SENB BM	BM	210	729	804	0.119	0.046
SENB WM	WM	210	741	833	0.048	0.015
SENB HAZ	HAZ	210	745	855	0.121	0.011
	BM	210	735	820	0.162	0.068

During the simulation of the welded joint material's fracture behavior, the applied load P is plotted against the Crack Mouth Opening Displacement (CMOD) for the regions BM, WM, and HAZ. The numerical curves and experimental P-CMOD curves obtained from the experimental three-point bending testing SENB specimens are plotted in graph in Fig. 11. The results show that the lowest fracture resistance occurs in BM, with a maximum load P = 8.73 kN at CMOD = 0.633 mm. The highest fracture resistance is observed in HAZ, reaching P = 15.54 kN at CMOD = 0.803 mm. The WM region exhibits an intermediate resistance, with an average load of P = 11.85 kN at a CMOD = 0.285 mm, shown in Table 6.

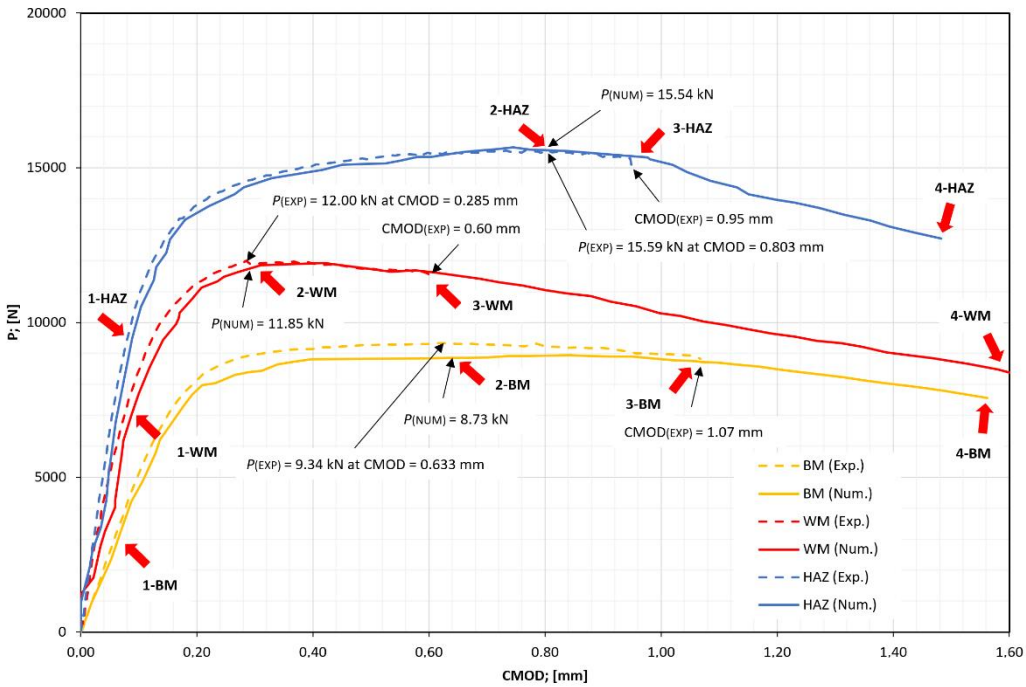

Fig. 11 SENB specimens for BM, WM and HAZ – P-CMOD numerical and experimental curves

Table 6 SENB specimens for BM, WM and HAZ – *P*-CMOD numerical and experimental values

Specimen	Material	$P_{max.\ (exp.)}$ [kN]	$P_{max.\ (num.)}$ [kN]	$P_{max.\ (diff.)}$ [%]	$CMOD_{Pmax.}$ [mm]	$CMOD_{max.\ (exp.)}$ [mm]
SENB BM	BM	9.34	8.73	6.75	0.633	1.07
SENB WM	WM	12.00	11.85	1.26	0.285	0.60
SENB HAZ	HAZ/BM	15.59	15.54	0.32	0.803	0.95

Numerical curves show good matching with the experimental ones, demonstrating the potential of numerical methods to predict the fracture behavior of heterogeneous welded structures.

The stress state and fracture behavior at specific loading points in the *P*-CMOD curves for each numerically derived representation, including BM, WM, and HAZ samples, is illustrated in Fig. 12, with characteristic points chosen for demonstration.

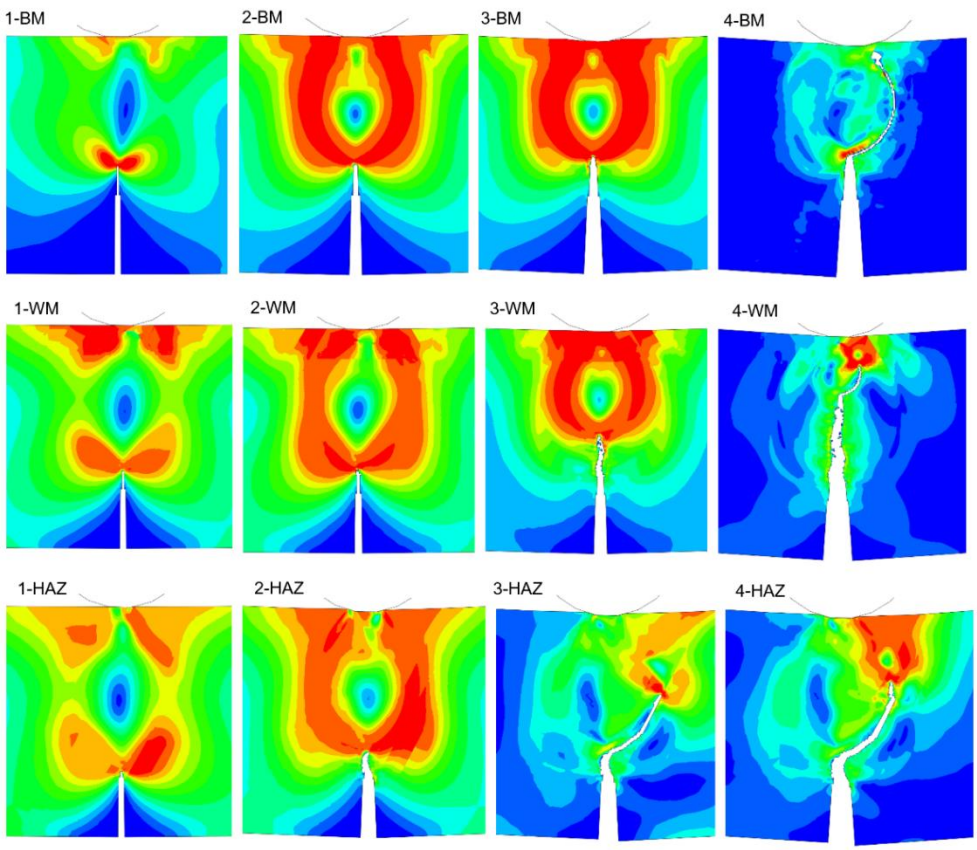

Fig. 12 *P*-CMOD numerical curves for BM, WM and HAZ – characteristic points

Characteristic to specimen curves, the loading point 1 shows the specific stress field at crack tip, prior to crack initiation. Point 2 correlates with $P_{max.}$ value on curves. Past this point, the crack growth continues at point 3, with final specimen failure at point 4. In case of BM and WM, the crack grows in vertical direction, until the sudden collapse. In case of HAZ it can be observed that crack starts the vertical growth through HAZ region, followed by directional change along the BM/HAZ boundary, until the final failure.

Comparing the numerically obtained physical fracture crack (PFC) size a_p with the actual ones from the experimental testing, it can be observed their good qualitative matching. The actual measured values are: for BM a_p = 7.499 mm, for WM a_p = 5.861 mm and for HAZ a_p = 4.819 mm.

CONCLUSION

The heterogeneity inherent in welded joints can be effectively incorporated into computational simulations by employing appropriate representative numerical models. These models can encompass three primary weld zones: the base material (BM), the weld material (WM), and the heat-affected zone (HAZ). To make the models manageable and suitable for numerical analysis, certain simplifications of the actual weld geometry are necessary. These simplifications are carefully designed to retain the essential mechanical and geometric characteristics of the weld zones while reducing complexity. For the implementation of the simulations, SENB specimens were modeled, reflecting the real specimen geometry and critical regions of the weld joint. Utilizing the ductile damage material model, combined with tensile properties that were previously obtained through experimental testing of each material zone, enables a detailed simulation of the fracture behavior specific to each zone within the welded joint. These simulations produce fracture resistance curves, represented as *P*–CMOD (i.e. load versus crack mouth opening displacement) curves, which are comparable to experimental results. This approach allows for a comprehensive understanding of how heterogeneity affects fracture behavior, providing valuable insights for the design and assessment of welded structures.

ACKNOWLEDGMENT

Authors acknowledge the Slovenian Research Agency ARRS for partly funding this investigation in frame of the research program P2-0137 “Numerical and Experimental analysis of Nonlinear Mechanical Systems”.

References

[1] K. E. EASTERLING: *Introduction to the Physical Metallurgy of Welding,* Second Edition, London, Butterworth-Heinemann, 1992.
[2] S. KOU: *Welding Metallurgy*, Second Edition, John Wiley and Sons, Hoboken, New Jersey, 2003.
[3] E. F. NIPPES: ‘The weld heat-affected zone’, *Weld. J.*, 38 (1), pp. 1-17, 1959.

[4] W. F. SAVAGE, E. F. NIPPES, E. S. SZEKERES: 'A Study of Weld Interface Phenomena in a Low Alloy Steel', *Weld. J.*, 55 (9), pp. 260-268, 1976.
[5] J. C. LIPPOLD: *Welding Metallurgy and Weldability*, John Wiley & Sons, Inc., Hoboken, New Jersey, 2015.
[6] M. LOMOZIK: 'Effect of the welding thermal cycles on the structural changes in the heat affected zone and on its properties in joints welded in low-alloy steels', *Weld. Int.*, 14, pp. 845-850, 2000, doi: 10.1080/09507110009549281.
[7] M. KOÇAK, M. ES-SOUNI, L. CHEN, K.-H. SCHWALBE: 'Microstructure and weld metal matching effects on HAZ toughness', *Proc. of the 8th Int. Conf. OMAE-ASME*, The Hauge, Netherlands, p.p. 623-633, March 19-23 1989.
[8] J. SPURRIER, P. HANCOCK, J. P. CHUBB: 'An assessment of weld mis-matching', *Engineering Fracture Mechanics*, Volume 53, Issue 4, pp. 581-592, 1996, https://doi.org/10.1016/0013-7944(95)00180-8.
[9] Y. LEI, R. A. AINSWORTH: 'Failure assessment diagrams for cracks in welds with mismatched mechanical properties', American Society of Mechanical Engineers (ASME) *pressure vessels and piping conference*, Montreal, Canada, 21-26 Jul 1996, pp. 65-73, 1996.
[10] Y. J. KIM, K. H. SCHWALBE: 'Compendium of yield load solutions for strength mismatched SE(T), SE(B) and C(T) specimens', *Eng. Fract. Mech.* 68, pp. 1137-1151, 2001.
[11] Y. J. KIM, K. H. SCHWALBE: 'Mismatch effect on plastic yield loads in idealized weldments–I: weld centre cracks', *Eng. Fract. Mech.* 68, pp. 163-182, 2001.
[12] Y. J. KIM, K. H. SCHWALBE: 'Mismatch effect on plastic yield loads in idealized weldments–II: heat affected zone cracks', *Eng. Fract. Mech.* 68, pp. 183-199, 2001.
[13] G. H. B. DONATO, R. MAGNABOSCO, C RUGGIERI: 'Effects of weld strength mismatch on J and CTOD estimation procedure for SE(B) specimens', *Int. J. Fract.* 159, pp. 1-20, 2009,
[14] U. ZERBST, R. A. AINSWORTH, H. TH. BEIER, H. PISARSKI, Z. L. ZHANG, K. NIKBIN, T. NITSCHKE-PAGEL, S. MÜNSTERMANN, P. KUCHARCZYK, D. KLINGBEIL: 'Review on fracture and crack propagation in weldments – A fracture mechanics perspective', *Engineering Fracture Mechanics*, 132, pp. 200-276, 2014, 10.1016/j.engfracmech.2014.05.012 .
[15] D. TOMERLIN, N. GUBELJAK, D. KOZAK: 'Gleeble Simulation of HAZ in S690QL Steel: Microstructural and Mechanical Properties', *Key engineering materials*, 966, pp. 115-120, 2023, doi: 10.4028/p-HmvK3N.
[16] D. TOMERLIN, D. KOZAK, L. FERLIČ, N. GUBELJAK: 'Experimental and Numerical Analysis of Fracture Mechanics Behavior of Heterogeneous Zones in S690QL1 Grade High Strength Steel (HSS) Welded Joint', *Materials* 16 (2023) 6929, https://doi.org/10.3390/ma16216929.
[17] D. TOMERLIN, D. KOZAK, N. GUBELJAK, I. PENTEK: 'Tensile testing of S690QL1 HSS welded joint heterogeneous zones using small scale specimens and indentation methods', *Materials Testing* 66(10), pp. 1600-1619, 2024, https://doi.org/10.1515/mt-2024-0136
[18] D. TOMERLIN, D. KOZAK, N. GUBELJAK, M. MAGIĆ KUKULJ: 'Stress-strain properties of HSS steel welded joint heterogeneous structure: experimental and numerical evaluation', *Mathematical Modelling of Weld Phenomena 13*, Verlag der Technischen Universität Graz, 2023, doi:10.3217/978-3-85125-968-1-23
[19] Fine-Grain Structural Steels MAXIL® 690, Ilsenburger Grobblech, 2019.
[20] BÖHLER X 70-IG - Solid wire, low-alloyed, high strength, Böhler Welding by Voestalpine; 2014.
[21] S. HERTELÉ, W. DE WAELE, M. VERSTRAETE, R. DENYS, N. O'DOWD: 'J-integral analysis of heterogeneous mismatched girth welds in clamped single-edge notched tension specimens', *Int. J. Press. Vessel. Pip.* 119, pp. 95-107, 2014.

[22] P. ŠTEFANE, S. HERTELÉ, S. NAIB, W. DE WAELE, N. GUBELJAK: 'Effects of Fixture Configurations and Weld Strength Mismatch on J-Integral Calculation Procedure for SE(B) Specimens', *Materials* 15, 962, 2022.
[23] L. STARČEVIČ, N. GUBELJAK, J. PREDAN: 'The Numerical Modelling Approach with a Random Distribution of Mechanical Properties for a Mismatched Weld', *Materials*, 14, 5896, 2021
[24] S. HERTELÉ, N. O'DOWD, K. VAN MINNEBRUGGEN, M. VERSTRAETE, W. DE WAELE: 'Fracture Mechanics Analysis of Heterogeneous Welds: Validation of a Weld Homogenisation Approach', *Procedia Mater. Sci.* 3, pp. 1322-1329, 2014.
[25] Y. BI, X. YUAN, M. HAO, S. WANG, H. XUE: 'Numerical Investigation of the Influence of Ultimate-Strength Heterogeneity on Crack Propagation and Fracture Toughness in Welded Joints', *Materials*, 15, 3814, 2022
[26] D. N. I. ALVES, J. G. ALMEIDA, M. C. RODRIGUES: 'Experimental and numerical investigation of crack growth behavior in a dissimilar welded joint', *Theor. Appl. Fract. Mech*. 109, 102697, 2020.
[27] ABAQUS: *Abaqus/Explicit User's Manuals*, Version 6.11, Dassault Systèmes Simulia Corp. Providence, RI, USA, 2011.
[28] ABAQUS DUCTILE DAMAGE MODEL: available online: https://abaqus-docs.mit.edu/2017/English/SIMACAEMATRefMap/simamat-c-damageevolductile.htm.
[29] F. YANG, M. VELJKOVIC, Y. LIU: 'Ductile damage model calibration for high-strength structural steels', *Constr. Build. Mater.* 263, 120632, 2020.
[30] W. SONG, X. LIU, F. BERTO, J. XU, H. FANG: 'Numerical simulation of prestrain history effect on ductile crack growth in mismatched welded joints', *Fatigue Fract. Eng. Mater. Struct.* 40, pp. 1472-1483, 2017.
[31] Y. CHO, C. LEE, J.-J. Yee, D.-K. Kim: 'Modeling of Ductile Fracture for SS275 Structural Steel Sheets', *Appl. Sci.*, 11, 5392, 2021, https://doi.org/10.3390/app11125392.
[32] H. XIN, J. A. F. O. CORREIA, M. VELJKOVIC, F. BERTO: 'Fracture parameters calibration and validation for the high strength steel based on the mesoscale failure index', *Theor. Appl. Fract. Mech.* 112, 102929, 2021.
[33] U. ZERBST, M. MADIA, B. SCHORK, J. HENSEL, P. KUCHARCZYK, D-T. NGOULA, D. TCHUINDJANG, J. BERNHARD, C. BECKMANN: *Fatigue and fracture of weldments. The IBESS approach for the determination of the fatigue life and strength of weldments by fracture mechanics analysis*, Springer, Cham, Switzerland, 2019.
[34] U. ZERBST: 'Application of fracture mechanics to welds with crack origin at the weld toe: a review Part 1: Consequences of inhomogeneous microstructure for materials testing and failure assessment', *Weld World* 63, pp.1715-1732, 2019, https://doi.org/10.1007/s40194-019-00801-5.
[35] A. SEDMAK, E. DONCHEVA, B. MEDJO, M. RAKIN, N. MILOSEVIC, D. RADU: 'Crack Size and Undermatching Effects on Fracture Behavior of a Welded Joint', *Materials* 16 (13):4858, 2023, doi: 10.3390/ma16134858. PMID: 37445171; PMCID: PMC10343383.